Comparative transcriptome analysis of astaxanthin accumulation difference between non-motile cells and akinetes of Haematococcus pluvialis

Lei Fang
State Key Laboratory of Bioreactor Engineering, East China University of Science and Technology, Shanghai 200237, People's Republic of China

Jingkui Zhang
State Key Laboratory of Bioreactor Engineering, East China University of Science and Technology, Shanghai 200237, People's Republic of China

Zhongnan Fei
State Key Laboratory of Bioreactor Engineering, East China University of Science and Technology, Shanghai 200237, People's Republic of China

Minxi Wan (wanminxi@ecust.edu.cn)
East China University of Science and Technology

Research

Keywords: Astaxanthin, Haematococcus pluvialis, Lipid, Photosynthesis, Transcriptome

Posted Date: May 11th, 2020

DOI: https://doi.org/10.21203/rs.3.rs-25722/v1

Comparative transcriptome analysis of astaxanthin accumulation difference between non-motile cells and akinetes of *Haematococcus pluvialis*

Lei Fang, Jingkui Zhang, Zhongnan Fei, Minxi Wan*

State Key Laboratory of Bioreactor Engineering, East China University of Science and Technology, Shanghai 200237, People's Republic of China.

* Address correspondence to Minxi Wan, wanminxi@ecust.edu.cn.

Minxi Wan, Ph.D, Address: Mail box 301, Meilong Road 130, Shanghai 200237, People's Republic of China. Tel. /fax: +86-21-64252104

Abstract

Background: Nature astaxanthin is mainly derived from *Haematococcus pluvialis*. *H. pluvialis* has four kinds of cell morphology. Based on sequential heterotrophy-dilution-photoinduction (SHDP) technology, photoinduction using non-motile cells as seeds could result in a higher astaxanthin production than that of using brown akinetes as photoinduction seeds. To have a comprehensive understanding of this phenomenon, transcriptome analysis was conducted in this study.

Results: Though most of photosynthesis genes expression were down-regulated during the SHDP culture process. Comparing with the group using brown akinetes as photoinduction seeds, the genes expression involved in astaxanthin biosynthesis, lipid biosynthesis and photosynthesis were up-regulated in the non-motile cells group. Especially, *chyb* gene improving the conversion of *β*-carotene into astaxanthin was up-regulated by 2.6-fold. The *acaca* gene enhancing the carboxylation of acetyl-CoA to malonyl-CoA was up-regulated by 1.4-fold.

Conclusions: Astaxanthin synthesis mechanism of non-motile cells with higher astaxanthin accumulation ability than brown akinetes was attributed to the up-regulation of astaxanthin metabolism, lipid metabolism and photosynthesis-related genes expression. The results are expected to guide the optimization of astaxanthin production in *H. pluvialis* by improving lipid content or photosynthesis.

Keywords Astaxanthin; *Haematococcus pluvialis*; Lipid; Photosynthesis; Transcriptome

Introductions

Astaxanthin is a non-vitamin A source of carotenoids. Its antioxidant activity is 10, 65, 100 and 550 folds higher than that of β-carotene, vitamin C, α-tocopherol, and vitamin E, respectively (Koller et al. 2014). Under certain light intensity and nitrogen deficiency conditions, *Haematococcus pluvialis* can accumulate astaxanthin up to 4% ~ 5% of dry weight (He et al. 2007). Therefore, *H. pluvialis* is recognized as the best source of natural astaxanthin. Industrial production of *H. pluvialis* was successfully achieved with a two stages model. First stage is cell proliferation phase, in which the algae cells grow rapidly to a high cell density. The second stage is photoinduction stage, aiming to promote *H. pluvialis* accumulating astaxanthin under strong light, high salinity or other extreme environments (He et al. 2007).

H. pluvialis has four kinds of cell morphology, e.g., spores (green, round or elliptical cells, unable to swim, cell diameter less than 10 μm), motile cells (green, elliptical cells, able to swim, cell diameter about 3~19 μm), non-motile cells (green, round cells, unable to swim, cell diameter about 19~40 μm) and akinetes (brown (low astaxanthin content) or red (high astaxanthin content), round cells, unable to swim, cell diameter about 30~60 μm). Although the recent study has implied that the appropriate cell morphology for photoinduction was the non-motile cells obtained from photoautotrophic culture (Li et al. 2019). The molecular mechanism underpinning the intricate astaxanthin biosynthetic pathway has not been explored.

The sequential heterotrophy-dilution-photoinduction (SHDP) technology of *H. pluvialis* was established by our research group with its own intellectual property rights (Wan et al., 2015). Cells were first cultivated heterotrophically to achieve a high cell density, then were diluted to a suitable concentration and switched to a favorable environment for cells acclimation. Finally, the culture was transferred to high light environment for

50 astaxanthin accumulation (Wan et al., 2015). Based on this technology, the photoinduction difference between non-
51 motile cells and akinetes of *Haematococcus pluvialis* was investigated, and then the molecular mechanisms
52 underlying the astaxanthin biosynthetic pathway and regulation were dissected in *H. pluvialis.*

53 **Materials and Methods**

54 **Algal strains**

55 *Haematococcus pluvialis* ZY-18 was obtained from State Key Laboratory of Bioreactor Engineering, East China
56 University of Science and Technology (Shanghai, China).

57 **Culture conditions**

58 The basic seed medium and culture methods were the same with Hata et al. (2001). The *H. pluvialis* cells were
59 obtained from broths at 250 h and 550 h. *H. pluvialis* cells was used for the next step in photoinduction experiments.

60 **Photoinduction conditions**

61 Cells from proliferation phase were inoculated to the NIES-N medium (Kang et al. 2005) and turned into the
62 photoinduction stage. The initial cell concentration was approximately 0.3 g/L in all the experiments. 1 L column
63 bioreactors (height: 45 cm, & diameter: 7 cm) were used for cells photoinduction. And the bioreactor was a
64 cylindrical glass tube with a conical bottom (height: 6 cm). 5% CO_2 mixing was conducted by sparing air
65 supplemented with a flow rate of 0.2 L/min. A gas sparger was centrally placed at the bottom. Throughout the
66 experiment, the light intensity was about 540 μmol/ (m_2·s) and the culture temperature was controlled at 28°C.

67 **Measurement of dry weight**

68 V ml broth containing algal cells was obtained by centrifuging the culture at 2,683 × g for 10 min, and collected into

69 an empty tumbler (W_1) after being washed twice with distilled water, and then dried at 85°C for 24 h (W_2) to weight.

70 The dry weight was calculated in terms of the equation:

71 $$C_x = (W_2\text{-}W_1)/V \times 1000 \quad (1)$$

72 Where C_x (g/L) is dry weight of broth, W_1 is the weight of the empty tumbler, and W_2 (g) is the weight after being

73 dried, and V (ml) is the volume of the initial sample, respectively.

74 **Determination of astaxanthin content**

75 The astaxanthin content was measured by a modified Boussiba method. V ml culture sample was centrifuged for 10

76 min at 2,683 × g. 4-6 pieces of glass beads and 1 ml of dimethyl sulfoxide were added to each centrifuge tube, and

77 subsequently were vortex oscillated for 30 s, and then heated with 45°C water bathing for 15 min. Later, 1 ml

78 acetone was added into the mixture solution and centrifuged for 10 min at 2,683 × g. Then the supernatant was

79 collected and transferred into a volumetric flask. Above mentioned acetone extraction and supernatant collection

80 were conducted repeatedly until the supernatant becomes transparent and the precipitate becomes white. The

81 absorbance values of the extracts were determined at 474 nm using acetone as reference.

82 The astaxanthin content was calculated in terms of the equation:

83 $$C_{Car} = OD_{474} \times V_1 / V_2 \times Dilution\ ration/210 \quad (2)$$

84 $$C_{Asta\ content} = C_{car} / C_x \times 85\% \quad (3)$$

85 where C_{Car} is the concentration of carotenoid (mg/L), Cx is the dry weight of the algal (g/L) and $C_{Asta\ content}$ is the

86 content (%) of astaxanthin, V_1 is the volume of the volumetric flask (ml), and V_2 is the volume of the initial sample

87 (ml).

RNA isolation, cDNA library preparation, and sequencing

Totally, the transcription profiling of samples at six time points were evaluated (Fig.1). In the proliferation stage, three samples in different time points were selected: (1) Sample 1: heterotrophic culture cells at 100 h (H 100h, green motile cells accounted for the vast majority); (2) Sample 2: heterotrophic culture cells at 250 h (H 250h, green non-motile cells accounted for the vast majority); (3) Sample 3: heterotrophic culture cells at 550 h (H 550h, brown akinetes accounted for the vast majority, astaxanthin content was low). In the photoinduction phase, three samples were also selected as follows: (1) Sample 4: Sample 2 cells were transferred to weak light for 0.5 d under photoinduction condition (P 0.5d, green non-motile cells were converted to brown akinetes); (2) Sample 5: Sample 3 cells were transferred and exposed to weak light for 6 days under photoinduction condition (P 6d, red akinetes accounted for the majority, astaxanthin content was high, and astaxanthin content was no longer increased); (3) Sample 6 was the Sample 2 cells continued photoinduction until the 6_{th} day (P 6d, red akinetes account for the vast majority. The astaxanthin content was high, was no longer to increase, and was higher than that of sample5). Therefore, there are two cultivation routes named treatment group (green non-motile cells were used for photoinduction, in the order: Sample 1, Sample 2, Sample 4 and Sample 6) and control group (brown akinetes were used for photoinduction, in the order: Sample 1, 2, Sample 3 and Sample 5), with two biological replicates at each time point.

Total RNA of each sample was extracted and mRNA was purified. Then the cDNA library was constructed and subjected to paired-end (PE) sequencing based on the Illumina NextSeq500 sequencing platform by Shanghai Personal Biotechnology Company. All sequencing data reported in this paper have been deposited in the National

Omics Data Encyclopedia (NODE, https://www.biosino.org/node/). The accession numbers for RPKM (Reads Per Kilobase per Million mapped reads) and annotation results are NODE: OEP000493.

Transcriptome mapping, annotation, and differential transcription analysis

The software of cut-adapt was used to remove adapters, poly-N strands, and low quality reads. Then all filtered reads were examined by FastQC (http://www.bioinformatics.babraham.ac.uk/projects/fastqc/) to confirm data quality. Transcript assembly were used Trinity with a K-mer 25 bp. Every transcript was compared with the NCBI non-redundant protein database and eggNOG (evolutionary genealogy of genes: non-supervised Orthologous Groups) using the Blast algorithm (version 2.2.30+). Transcripts with same gi number were classified as a unigene and only the longest transcript was kept. After that, filtered reads were mapped to unigenes with Bowtie2 (v2.2.4) and the reads per kilobase of exon model per million (RPKM) mapped fragments was used to represent gene expression.

Differential transcription analysis between samples was conducted using the R package, DEGseq (version 1.18.0). Genes with $|\text{fold changes}| > 2$ and $P\text{-value} < 0.05$ were considered as statistically significant. Functional analysis of differential transcription genes was performed by Gene ontology (GO) and Kyoto Encyclopedia of Genes and Genomes (KEGG) enrichment analysis. GO analysis of each unigene was carried out using Blast2go software and KEGG enrichment analysis was performed using KASS and KEGG automatic annotation sever, respectively.

Statistical analysis

Statistical analyses were performed using the Spearman correlation analysis (SPSS19.0). For all of the data analysis, a $P\text{-value} < 0.05$ was considered as statistically significant.

Results and discussion

The comparison of photoinduction differences between Non-motile cells and Akinetes

Scanning electron microscope (SEM) and transmission electron microscope (TEM) images of *H. pluvialis* were carried out during culture process to explore the changes of different cells morphology (Fig. 1). From the TEM images, more lipid drops were observed with non-motile cells as seeds at the end of photoinduction (1246 SHDP route). Cheng et al. (2017) reported that massive astaxanthin was esterified in the endoplasmic reticulum, and deposits in cytoplasmic lipid droplets to avoid the feedback inhibitor of carotenoids biosynthesis. Thus, non-motile cells may have much more astaxanthin accumulation ability.

To verify the above conclusion, the astaxanthin content and concentration were detected. Comparing with the brown akinetes group, a better photoinduction result was acquired using non-motile cells as seeds (Fig. 2). The astaxanthin content and concentration of non-motile cells group were 3.40 ± 0.03% and 25.7 ± 1.54 mg/L, respectively (Fig. 2), which were 69.58% and 87.88% higher than those in brown akinetes group, respectively. Li et al. (2019) also demonstrated that the appropriate cell morphology for photoinduction was the non-motile cells.

Transcriptome and pathway analysis involved in lipid metabolism

To understand comprehensively non-motile cells with better ability of astaxanthin accumulation, transcriptome analysis was conducted. The direct precursor of fatty acid biosynthesis is acetyl-CoA. Acetyl-CoA carboxylase (ACACA) can enhance the carboxylation of acetyl-CoA to malonyl-CoA. This step was considered a critical step in the FA-biosynthetic pathway (Huerlimann and Heimann 2013). Cheng et al. (2017) has reported that the up-regulation of *acaca* gene could enhance fatty acid biosynthesis, thus promoting astaxanthin esterification and deposition. Compared with control, *acaca* gene was up-regulated by 1.4-fold at the end of photoinduction (Table

1). Thus, fatty acid synthesis and astaxanthin esterification was further improved. *FabD* ([acyl-carrier-protein] S-malonyltransferase) ,improving the formation of malonyl-ACP from malonyl-CoA, was also up-regulated by 1.4-fold at the end of photoinduction compared with control (Table 1). FabH (3-oxoacyl-[acyl-carrier-protein] synthase III), which catalyzes the condensation between acetyl-CoA and malonyl-ACP to form acetoacetyl-ACP, was up-regulated by 1.8-fold (Table 1). Malomyl-ACP was catalyzed to (R)-3-Hydroxy-butanoyl-ACP by FabF (3-oxoacyl-[acyl-carrier-protein] synthase II) and FabG (3-oxoacyl- [acyl-carrier protein] reductase). *fabG* gene transcription was up-regulated in both routes when akinetes formation (Fig. 3a,b). However, *fabF* gene expression was only up-regulated in the treatment group when akinetes formation (Fig. 3a,b). Hexadecenoic acid and Octadecanoic acid synthesis can be catalyzed by FATA. *fata* gene expression level was significantly increased by 2.2-fold (Fig. 3c).

Compared with the control, all genes related in lipid metabolism were up-regulated (Fig. 3c and Table 1). The results proved that astaxanthin synthesis was positively correlated with lipid synthesis. Transcriptome analysis explained the mechanism of non-mobile cells owning stronger ability of astaxanthin accumulation than brown akinetes.

Free form astaxanthin is unstable and easy to be oxidized. Esterified form astaxanthin can be synthesized, when the hydroxyl groups of free form astaxanthin are dehydrated and condensed with the carboxyl group of the fatty acid. Astaxanthin is lipophilic and needs to be dissolved in lipid. In addition, the lipid in the droplet form can protect BKT from being degraded by protein kinases (Solovchenko 2015). Thus, the strong ability of non-mobile cells to accumulate astaxanthin can be attributed to the improvement of lipid metabolism.

Transcriptome and pathway analysis involved in photosynthesis

Compared with brown akinetes, non-mobile cells have much more chlorophyll content. Therefore, the

166 photosynthesis-related genes expression difference between treatment group and control group was analyzed.

167 ATP synthesis is catalytic by ATP synthase subunit alpha (atpA). When akinetes formation, *atpA* gene was up-
168 regulated in both routes (Fig. 4a,b). Thus, akinetes formation may need ATP. However, except *atpA* gene, most of
169 photosynthesis-related genes transcription were down-regulated during the akinetes formation (Fig. 4a,b), e.g.,
170 photosynthetic energy absorption depends on light-harvesting chlorophyll protein complex (LHCs). The light-
171 harvesting complexes (LHCs), belonging to the photosynthesis-antenna proteins, were the first proteins and could
172 capture light energy quickly (Huang et al. 2019). LHC formation is catalytic by chlorophyll a-b binding protein 4
173 (Lhca5) and chlorophyll a-b binding protein CP29 (Lhcb4). Whereas, both *Lhca5* and *Lhcb4* genes expression were
174 down-regulated during akinetes formation (Fig. 4a,b). The down-regulated of *Lhc* genes expression may result in
175 the abnormal chloroplast development and the decrease of chlorophyll content (Wang et al. 2016).

176 Nonetheless, at the end of photoinduction, the photosynthesis genes expression level of treatment group were still
177 higher than that of the control group (Fig. 4c, d and Table 1). This results could further explain the strong ability of
178 non-mobile cells to accumulate astaxanthin.

179 Photosynthesis can convert light and carbon dioxide into glucose. Photosynthesis also provides ATP and NADPH
180 for cell growth and metabolism (Huang et al. 2019). Most photosynthetic carbon is directed toward carbohydrate
181 (Melis 2012). Accompanying by morphological and metabolic changes during akinetes formation of *H. pluvialis*,
182 photosynthetic carbons are reallocated from carbohydrate to protein, lipid, carotenoids, and nucleic acid (Cheng et
183 al. 2016). Thus, photosynthesis is important for microalgae growth and secondary metabolite synthesis. The strong
184 ability of non-mobile cells to accumulate astaxanthin can be attributed to the improvement of photosynthesis.

185 **The metabolic network of astaxanthin synthesis was proposed**

Based on the SHDP cultivation model and above transcriptome analysis results, the metabolic network of astaxanthin synthesis was proposed (Fig. 5). Astaxanthin synthesis ability was closely related to astaxanthin metabolism, lipid metabolism and photosynthesis.

The conversion of Geranylgeranyl–pp (GGPP) into astaxanthin synthesis is successively catalyzed by *β*-carotene ketolase (BKT), *β*-carotene-3-hydroxylase (CHYB), lycopene beta cyclase (LCYB), phytoene synthase (PSY) and *ζ*-Carotene desaturase (ZDS). These enzymes have been reported as essential enzymes in astaxanthin synthesis (Zhong et al. 2011). Comparing with brown akinetes group, the *bkt*, *chyb*, *lcyb*, *psy*, *zds* genes expression level were up-regulated by 1.9-fold, 2.6-fold, 1.9-fold, 2.4-fold, 2.0-fold, respectively (Table1). Thus, non-mobile cells have strong accumulate astaxanthin ability. Light energy, carbon dioxide and H_2O can be converted into glucose, ATP and NADPH through photosynthesis. Then glucose is converted into lipid (Melis 2012). Thus, the up-regulation of photosynthesis related genes can provide energy and carbon for the synthesis of glucose and lipid. Esterified form astaxanthin has strong antioxidant capacity, which was formed through the dehydration condensation between lipid and free astaxanthin (Karsten et al. 2009). Therefore, the increasing of lipid content is beneficial to astaxanthin synthesis. Above all, astaxanthin synthesis is closely related to astaxanthin metabolism, photosynthesis and lipid metabolism. The strong accumulate astaxanthin ability of non-mobile cells can be attributed to the improvement of astaxanthin metabolism, photosynthesis and lipid metabolism.

Conclusion

Based on SHDP technology, the metabolic network of astaxanthin synthesis was proposed. The astaxanthin synthesis mechanism of non-motile cells having higher astaxanthin accumulation ability than akinetes was attributed to the up-regulation of astaxanthin biosynthesis, lipid biosynthesis and photosynthesis related genes expression.

Abbreviations

DEGs: differentially expressed genes; NODE: National Omics Data Esncyclopedia; GGPP: geranylgeranyl-pp; SEM: scanning electron microscope; TEM: transmission electron microscope.

Acknowledgments

Not applicable.

Authors' contributions

M.W. and L.F. designed the study; L.F. analyzed the data and drafted the manuscript; J.Z. and Z.F. prepared the transcriptome sequencing samples and electron microscopy samples; M.W. reviewed and edited the article, and sought funding.

Funding

This research was funded by National Natural Science Foundation of China (31500062), China, Post Doctoral Science Foundation (2013M530183 & 2014T70400), China, and the Fundamental Research Funds for the Central Universities (222201414024), China. The authors declared that they have no conflicts of interest to this work.

Compliance with ethical standards

Availability of data and materials

The datasets supporting the conclusions of this article are included in the main manuscript file and additional files.

Ethics approval and consent to participate

Not applicable.

Consent for publication

Not applicable.

Conflict of interest

The authors declare that they have no conflict of interest.

References

Cheng J, Ke L, Yang Z, Zhou J, Cen K (2016) Enhancing the growth rate and astaxanthin yield of *Haematococcus pluvialis* by nuclear irradiation and high concentration of carbon dioxide stress: biomass, bioenergy, biowastes, conversion technologies, biotransformations, production technologies Bioresour Technol 204:49-54 doi:10.1016/j.biortech.2015.12.076

Cheng J, Li K, Zhu Y, Yang W, Zhou J, Cen K (2017) Transcriptome sequencing and metabolic pathways of astaxanthin accumulated in *Haematococcus pluvialis* mutant under 15% CO_2 Bioresour Technol 228:99-105 doi:10.1016/j.biortech.2016.12.084

Hata N, Ogbonna JC, Hasegawa Y, Taroda H, Tanaka H (2001) Production of astaxanthin by *Haematococcus pluvialis* in a sequential heterotrophic-photoautotrophic culture J Appl Phycol 13:395-402 doi:/10.1023/A:1011921329568

He P, Duncan J, Barber J (2007) Astaxanthin accumulation in the green alga *Haematococcus pluvialis*: effects of cultivation parameters J Integr Plant Biol 49:447-451 doi:10.1111/j.1744-7909.2007.00468.x

Huang L, Gao B, Wu M, Wang F, Zhang C (2019) Comparative transcriptome analysis of a long-time span two-step culture process reveals a potential mechanism for astaxanthin and biomass hyper-accumulation in *Haematococcus pluvialis* JNU35 Biotechno Biofuels 12:18-38 doi:10.1186/s13068-019-1355-5

Huerlimann R, Heimann K (2013) Comprehensive guide to acetyl-carboxylases in algae Crit Rev Biotechnol 33:49-65 doi:10.3109/07388551.2012.668671

Kang CD, Lee JS, Park TH, Sim SJ (2005) Comparison of heterotrophic and photoautotrophic induction on astaxanthin production by *Haematococcus pluvialis* Appl Microbiol Biotechnol 68:237-241

doi:10.1007/s00253-005-1889-2

Karsten H, Maximilian K, Jens R, Paul S, Graeme N, Klaus A (2009) Determination of astaxanthin and astaxanthin esters in the microalgae *Haematococcus pluvialis* by LC-(APCI)MS and characterization of predominant carotenoid isomers by NMR spectroscopy Anal Bioanal Chem 395:1613-1622 doi:10.1007/s00216-009-2837-2

Koller M, Muhr A, Braunegg G (2014) Microalgae as versatile cellular factories for valued products Algal Res 6:52-63

Li F et al. (2019) Accumulation of astaxanthin was improved by the nonmotile cells of *Haematococcus pluvialis* BioMed Res Int 2019:8101762 doi:10.1155/2019/8101762

Melis A (2012) Photosynthesis-to-fuels: From sunlight to hydrogen, isoprene, and botryococcene production Energy Environ Sci 5:5531-5539 doi:10.1039/C1EE02514G

Solovchenko AE (2015) Recent breakthroughs in the biology of astaxanthin accumulation by microalgal cell Photosynthesis Res 125:437-449 doi:10.1007/s11120-015-0156-3

Wan M, Zhang Z, Wang J, Huang J, Fan J, Yu A, Wang W, Li Y (2015) Sequential Heterotrophy–Dilution–Photoinduction Cultivation of *Haematococcus pluvialis* for efficient production of astaxanthin. Bioresour Technol 198:557-563

Wang L, Cao H, Chen C, Yue C, Hao X, Yang Y, Wang X (2016) Complementary transcriptomic and proteomic analyses of a chlorophyll-deficient tea plant cultivar reveal multiple metabolic pathway changes J Proteomics 130:160-169 doi:10.1016/j.jprot.2015.08.019

Zhong YJ et al. (2011) Functional characterization of various algal carotenoid ketolases reveals that ketolating

zeaxanthin efficiently is essential for high production of astaxanthin in transgenic *Arabidopsis* J Exp Bot 62:3659-3669

271 **Table 1**. Annotation and transcription changes of significantly different unigenes related to astaxanthin, fatty acid, pyruvate metabolic pathway and photosynthesis.

Gene name	Gene definition	KEGG	**Sample 5 (**brown akinetes photoinduction for 6 d**) vs Sample 6 (** non-mobile cells photoinduction for 6 d **)**	
			Fold change	***P*-value**
Astaxanthin biosynthesis pathway				
bkt	*β*-Carotene ketolase (EC 1.14.99.63)	K09836	1.9	***
chyb	*β*-Carotene 3-hydroxylase (EC 1.14.15.24)	K15746	2.6	***
lcyb	Lycopene beta cyclase (EC 5.5.1.19)	K06443	1.9	***
psy	15-cis-Phytoene/all-trans-phytoene synthase (EC 2.5.1.32)	K02291	2.4	***
zds	*ζ*-Carotene desaturase (EC 1.3.5.6)	K00514	2.0	***
Fatty acid metabolic pathway				
fata	Fatty acyl-ACP thioesterase A (EC 3.1.2.14)	K10782	2.2	***
acaca	Acetyl-CoA carboxylase/biotin carboxylase 1(EC 6.4.1.2)	K11262	1.4	***
fabF	3-Oxoacyl-[acyl-carrier-protein] synthase II (EC 2.3.1.179)	K09458	1.5	***

fabD	[Acyl-carrier-protein] S-malonyltransferase (EC 2.3.1.39)	K00645	1.4	***
fabH	3-Oxoacyl-[acyl-carrier-protein] synthase III (EC 2.3.1.180)	K00648	1.8	***
fabG	3-Oxoacyl-[acyl-carrier protein] reductase (EC 1.1.1.100)	K00059	2.1	***
Photosynthesis				
LHCB4	Chlorophyll a-b binding protein CP29	K08915	1.6	***
LHCA5	Chlorophyll a-b binding protein 4	K08911	1.5	***
atpA	ATP synthase subunit alpha (EC 7.1.2.2)	K02111	1.5	***
psbP	PsbP-like protein 1	K02717	1.4	***
psaE	Photosystem I reaction center subunit IV	K02693	1.1	*
psbO	Oxygen-evolving enhancer protein	K02716	1.1	*
psaO	Photosystem I subunit	K14332	1.1	*
psb28	Photosystem II reaction center PSB28 protein	K08903	1.1	*

*** indicates statistical significance at *P*-value $\leqslant$ 0.001; * indicates statistical significance at *P*-value $\leqslant$ 0.05.

Figure Legends

Fig. 1 Images of *H. pluvialis* cells at different time points. *H. pluvialis* images of control group (a) and treatment group (b) were conducted using scanning electron microscope (SEM, scale bar = 10 μm) and transmission electron microscope (TEM, scale bar = 5 μm), respectively. In both SHDP routes, sample 1 and sample 2 were the same heterotrophic sample at 100 h and 250 h, respectively. H 100 h, H 250 h and H 550 h represent heterotrophic culture for 100 h, 250 h and 550 h, respectively. P 0.5 d and P 6 d represent photoinduction for 0.5 d and 6 d, respectively. Blue arrow and red arrow represent heterotrophic culture and photoinduction, respectively

Fig. 2 Photoinduction effect of *H. pluvialis* using different cell morphology as seeds. (a) Astaxanthin content during photoinduction process, (b) Astaxanthin concentration during photoinduction process, (c) Dry weight during photoinduction process. Hollow circle represents green non-motile cells as photoinduction seeds, and solid square represents brown akinetes as photoinduction seeds. Data shown as mean ± SD, and number of replications is two (n = 2)

Fig. 3 RPKM and unigene transcript expression changes involved in lipid metabolism pathways of *H. pluvialis* when using non-mobile cells and brown akinetes as seeds. A/ B represents the RPKM changes involved in lipid metabolism pathways of *H. pluvialis* in control group (a) and the treatment group (b), respectively. In both SHDP routes, sample 1 and sample 2 were the same heterotrophic sample at 100 h and 250 h, respectively. H 100 h, H 250 h and H 550 h represent heterotrophic culture for 100 h, 250 h and 550 h, respectively. P 0.5 d and P 6 d represent photoinduction for 0.5 d and 6 d, respectively. Compared with control group, the gene expression change of the

291 treatment group were presented in KEGG pathway (c). Red represents gene expression was up-regulated. Data
292 shown as mean ± SD, and number of replications is two (n = 2)

293 **Fig. 4** RPKM and unigene transcript transcription changes involved in photosynthesis pathways of *H. pluvialis*
294 when using non-mobile cells and brown akinetes as seeds. A/B represents the RPKM changes associated with
295 photosynthesis in the control group (a) and the treatment group (b), respectively. In both SHDP routes, sample 1
296 and sample 2 were the same heterotrophic sample at 100 h and 250 h, respectively. H 100 h, H 250 h and H 550 h
297 represent heterotrophic culture for 100 h, 250 h and 550 h, respectively. P 0.5 d and P 6 d represent photoinduction
298 for 0.5 d and 6 d, respectively. Comparing with control group, the photosynthesis (c) and antenna protein (d) gene
299 expression changes of the experimental group were presented in KEGG pathway. Red represents gene expression
300 was up-regulated. Data shown as mean ± SD, and number of replications is two (n = 2)

301 **Fig. 5** The metabolic network and transcription regulation of astaxanthin metabolism. Deep red, light blue and dark
302 yellow background represent astaxanthin metabolism pathway, photosynthesis and lipid metabolism pathway,
303 respectively. Solid arrows indicate that the reaction proceeds continuously, dotted arrows indicate that intermediate
304 metabolites are omitted, and the number of 1, 2, 3, 4, 5, 6 represent Sample1 (Heterotrophic culture for 100 h,
305 Mobile cells), Sample 2 (Heterotrophic culture for 250 h, Non-mobile cells), Sample 3 (Heterotrophic culture for
306 550 h, Brown akinetes), Sample 4 (Sample 2 photoinduction for 0.5 d, Brown akinetes), Sample 5 (Sample 3
307 photoinduction for 6 d, Red akinetes), Sample 6 (Sample 2 photoinduction for 6 d, Red akinetes), respectively. The
308 number of replications is two (n = 2)

Figures

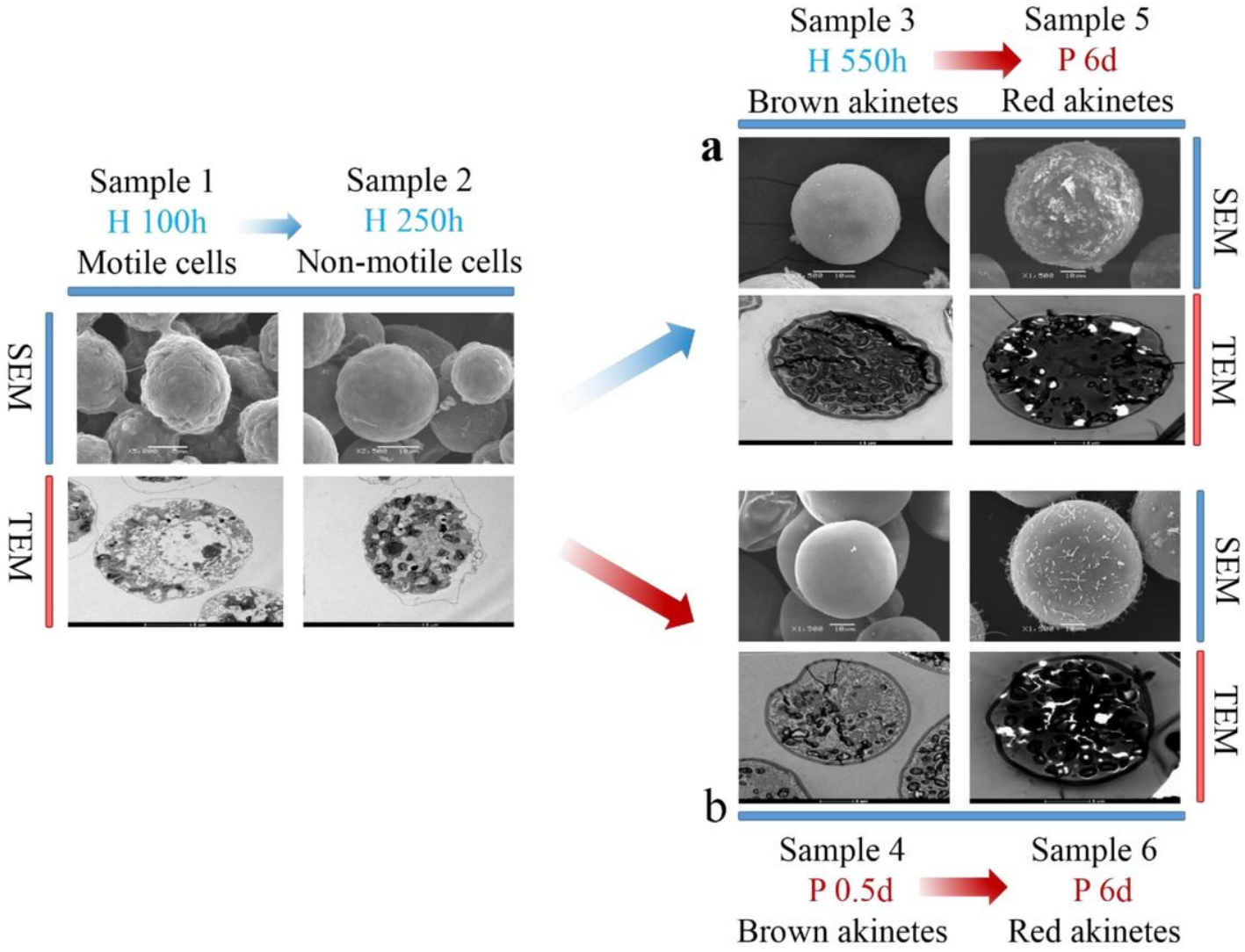

Figure 1

Images of H. pluvialis cells at different time points. H. pluvialis images of control group (a) and treatment group (b) were conducted using scanning electron microscope (SEM, scale bar = 10 μm) and transmission electron microscope (TEM, scale bar = 5 μm), respectively. In both SHDP routes, sample 1 and sample 2 were the same heterotrophic sample at 100 h and 250 h, respectively. H 100 h, H 250 h and H 550 h represent heterotrophic culture for 100 h, 250 h and 550 h, respectively. P 0.5 d and P 6 d represent photoinduction for 0.5 d and 6 d, respectively. Blue arrow and red arrow represent heterotrophic culture and photoinduction, respectively

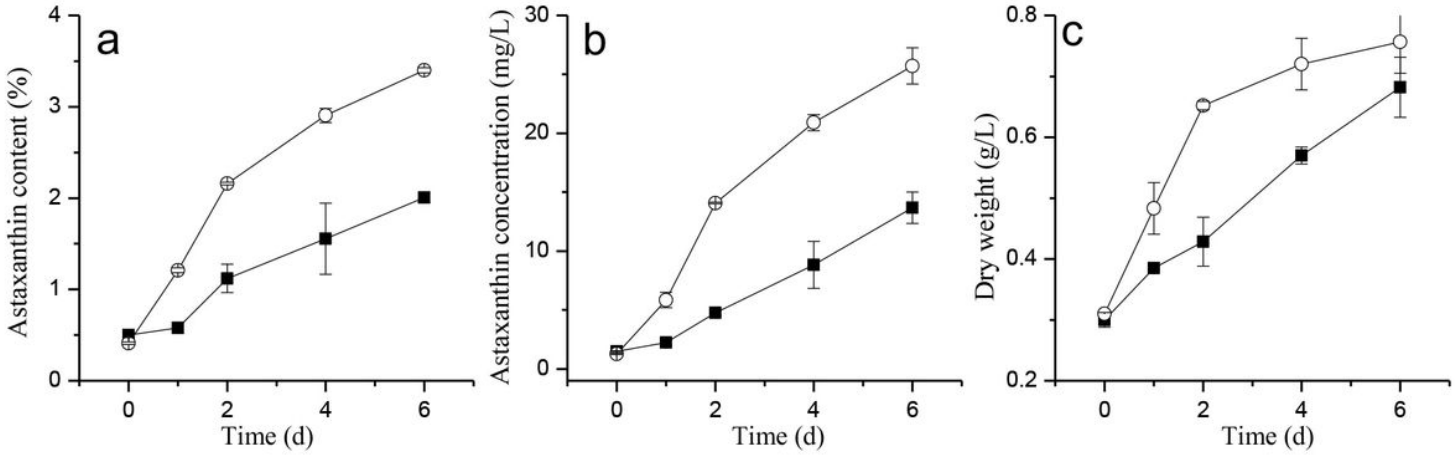

Figure 2

Photoinduction effect of H. pluvialis using different cell morphology as seeds. (a) Astaxanthin content during photoinduction process, (b) Astaxanthin concentration during photoinduction process, (c) Dry weight during photoinduction process. Hollow circle represents green non-motile cells as photoinduction seeds, and solid square represents brown akinetes as photoinduction seeds. Data shown as mean ± SD, and number of replications is two (n = 2)

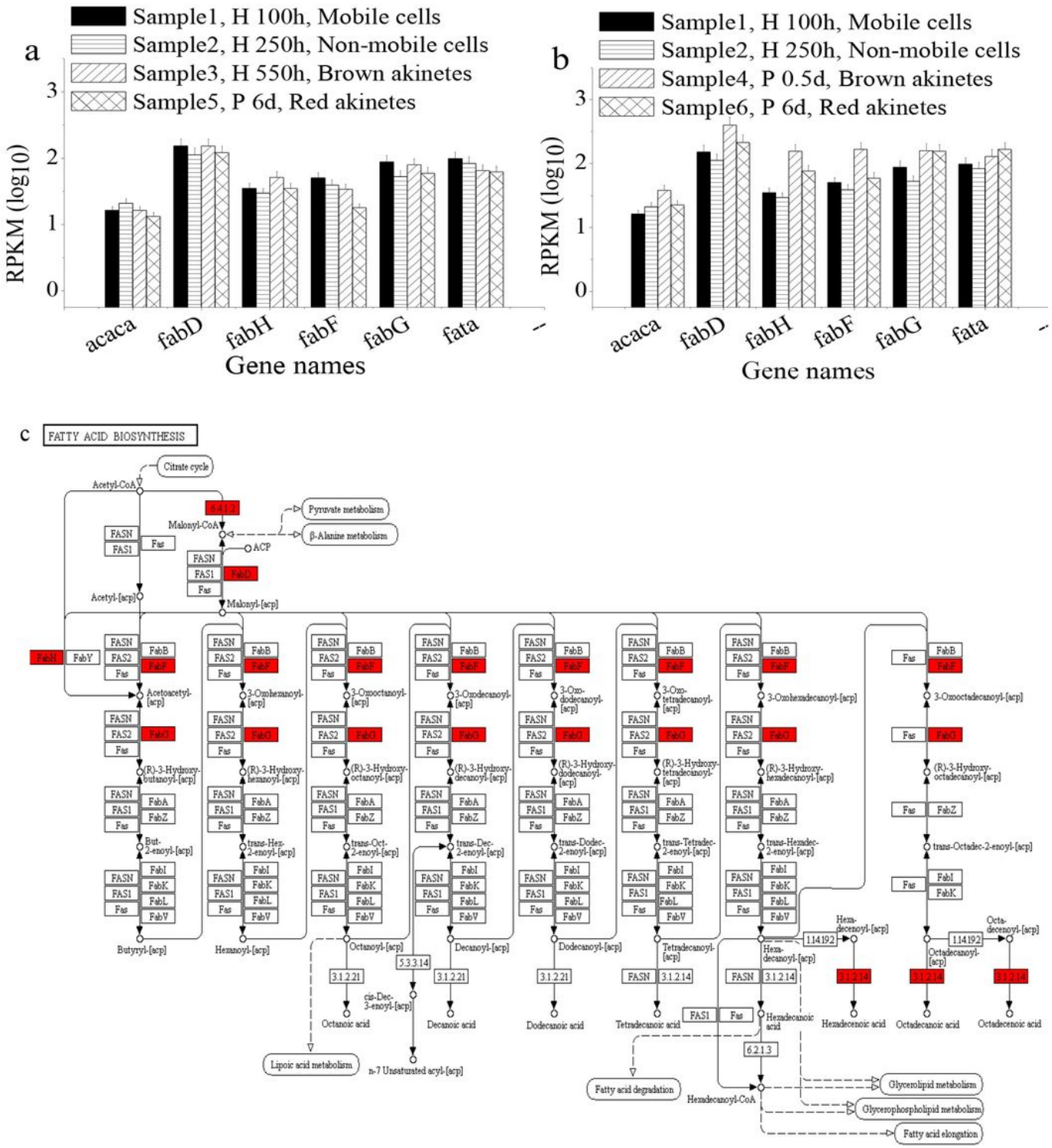

Figure 3

RPKM and unigene transcript expression changes involved in lipid metabolism pathways of H. pluvialis when using non-mobile cells and brown akinetes as seeds. A/ B represents the RPKM changes involved in lipid metabolism pathways of H. pluvialis in control group (a) and the treatment group (b), respectively. In both SHDP routes, sample 1 and sample 2 were the same heterotrophic sample at 100 h and 250 h, respectively. H 100 h, H 250 h and H 550 h represent heterotrophic culture for 100 h, 250 h and 550 h,

respectively. P 0.5 d and P 6 d represent photoinduction for 0.5 d and 6 d, respectively. Compared with control group, the gene expression change of the treatment group were presented in KEGG pathway (c). Red represents gene expression was up-regulated. Data shown as mean ± SD, and number of replications is two (n = 2)

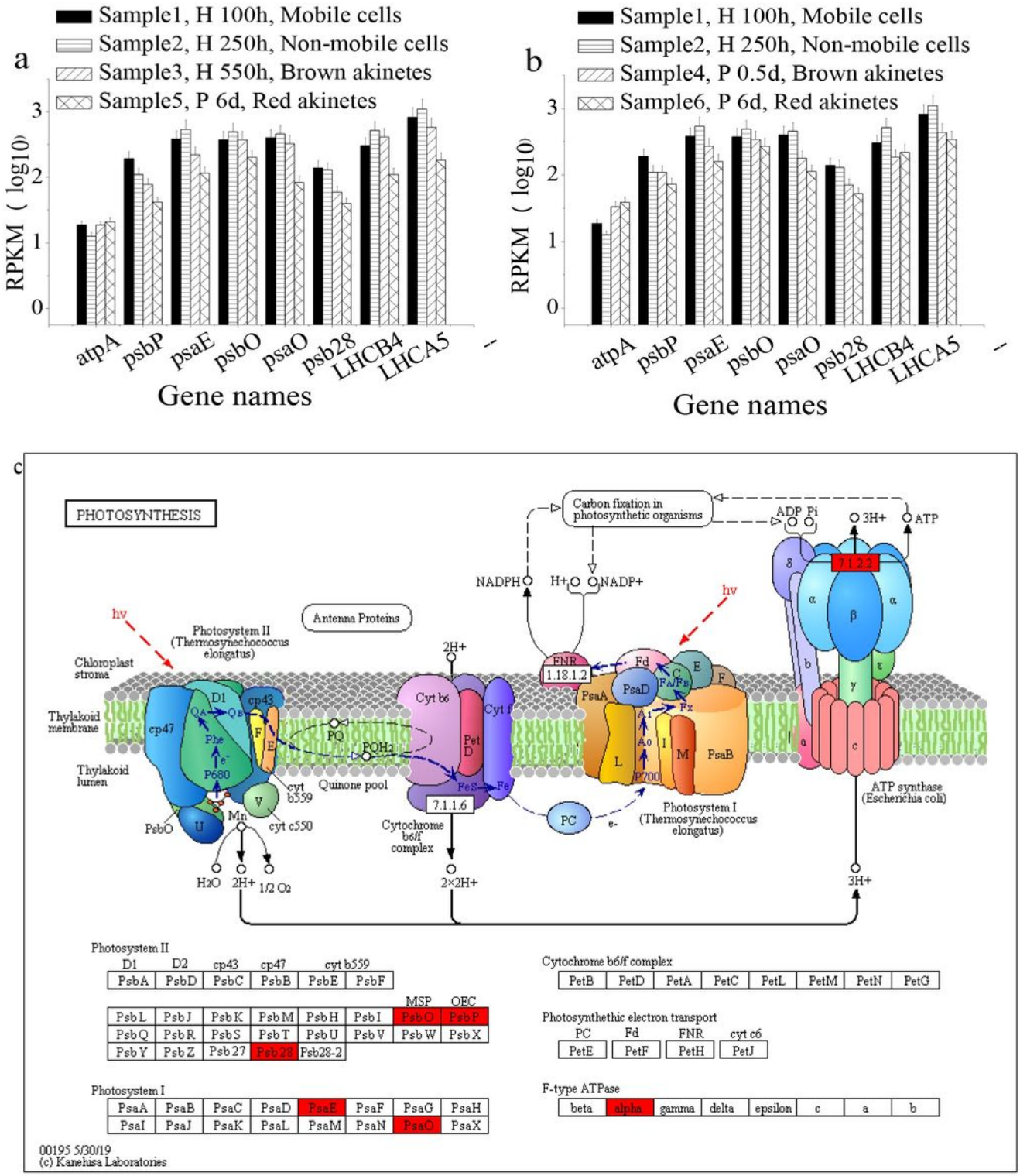

Figure 4

RPKM and unigene transcript transcription changes involved in photosynthesis pathways of H. pluvialis when using non-mobile cells and brown akinetes as seeds. A/B represents the RPKM changes associated with photosynthesis in the control group (a) and the treatment group (b), respectively. In both SHDP routes, sample 1 and sample 2 were the same heterotrophic sample at 100 h and 250 h, respectively. H 100 h, H 250 h and H 550 h represent heterotrophic culture for 100 h, 250 h and 550 h, respectively. P 0.5 d and P 6 d represent photoinduction for 0.5 d and 6 d, respectively. Comparing with control group, the photosynthesis (c) and antenna protein (d) gene expression changes of the experimental group were presented in KEGG pathway. Red represents gene expression was up-regulated. Data shown as mean ± SD, and number of replications is two (n = 2)

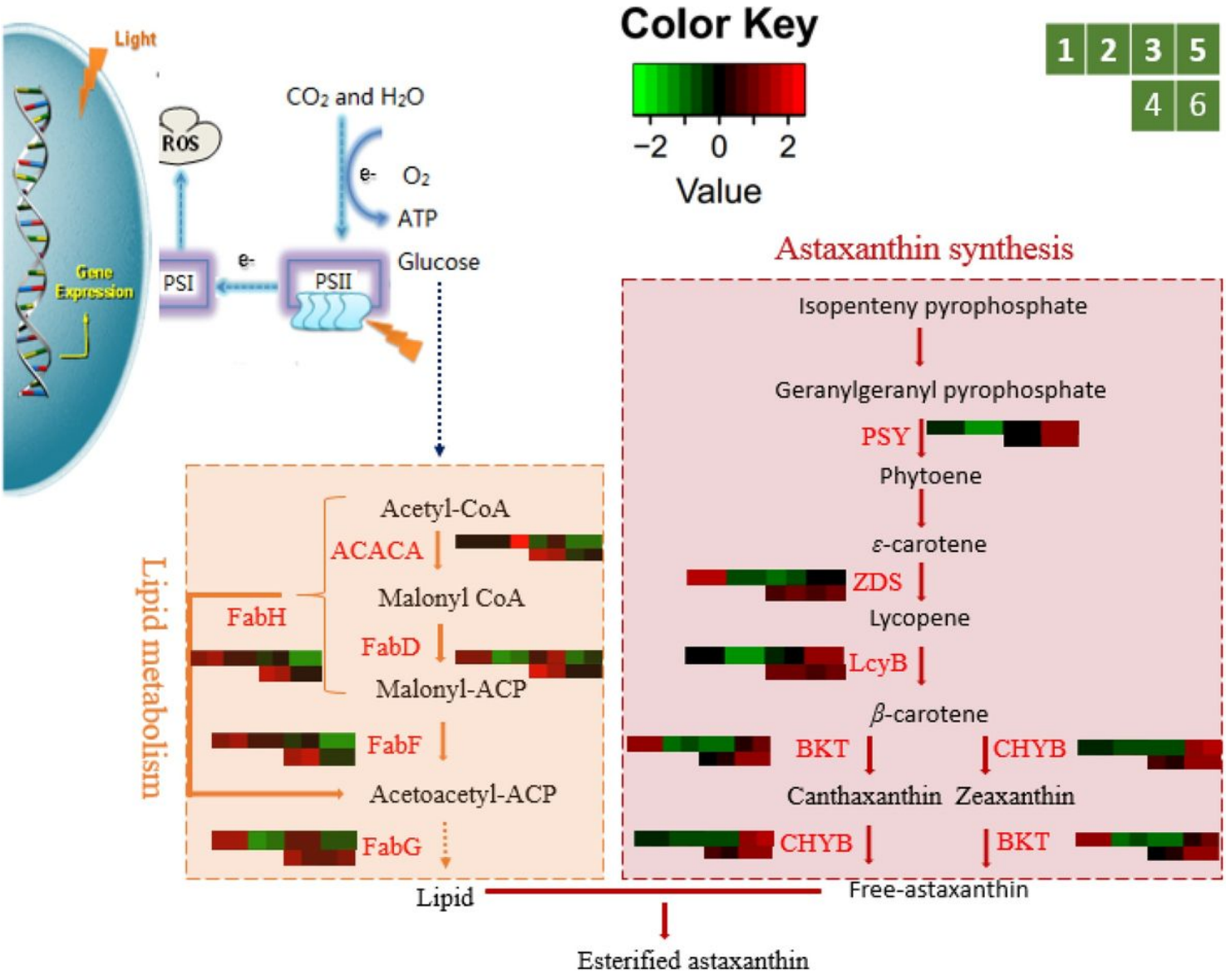

Figure 5

The metabolic network and transcription regulation of astaxanthin metabolism. Deep red, light blue and dark yellow background represent astaxanthin metabolism pathway, photosynthesis and lipid metabolism pathway, respectively. Solid arrows indicate that the reaction proceeds continuously, dotted

arrows indicate that intermediate metabolites are omitted, and the number of 1, 2, 3, 4, 5, 6 represent Sample1 (Heterotrophic culture for 100 h, Mobile cells), Sample 2 (Heterotrophic culture for 250 h, Non-mobile cells), Sample 3 (Heterotrophic culture for 550 h, Brown akinetes), Sample 4 (Sample 2 photoinduction for 0.5 d, Brown akinetes), Sample 5 (Sample 3 photoinduction for 6 d, Red akinetes), Sample 6 (Sample 2 photoinduction for 6 d, Red akinetes), respectively. The number of replications is two (n = 2)